Transactions, SMiRT-26
Berlin/Potsdam, Germany, July 10-15, 2022
Special Session: Impact Tests and Numerical Analyses

TEST PROGRAM AND NUMERICAL STUDIES ON REINFORCED CONCRETE SLABS IMPACTED BY LIQUID-FILLED MISSILES

Christian Heckötter[1], Ari Vepsä[2], Jürgen Sievers[3]

[1] Technical Expert, Gesellschaft für Anlagen- und Reaktorsicherheit (GRS) gGmbH, Cologne, Germany (christian.heckoetter@grs.de)
[2] Senior Scientist, VTT Technical Research Centre of Finland, Espoo, Finland
[3] Chief Expert Structure Mechanics, GRS, Cologne, Germany

ABSTRACT

Reinforced concrete (rc)-structures are used to protect vital parts of nuclear facilities against external hazards. These include malevolent or accidental airplane crash (APC). In this context kerosene mass may significantly contribute to loading as well as structural damage of the target rc-structure. Past research has been limited regarding this issue and few experimental data were available. Therefore, a test series called L-series dealing with impact of water-filled missiles on rc-slabs was carried out in the framework of Phase III of the multinational research project IMPACT at Technical Research Centre of Finland (VTT). In additional tests impact forces were recorded with a force plate system. Test results are used to validate numerical models for LS-DYNA and ANSYS AUTODYN software.

INTRODUCTION

Few test data on liquid filled missile impact on rc-structures are available. For instance, results of large-scale tests carried out at Sandia National Laboratories mentioned by Hessheimer and Dameron (2006) were published in a limited distribution report only. One objective of the VTT IMPACT project is to provide data for the validation of numerical tools. A description of the test facility is given by Lastunen et al. (2007). Previous experimental studies in IMPACT on liquid filled missiles were reported e.g. by Tarallo and Rambach (2013). The L-series carried out recently during Phase III of the IMPACT project at VTT (2019) addresses aspects which were not fully covered in previous tests, including:

- Influence of liquid and effects of partially filled tanks on load-time-functions (LTF)
- Influence of increased liquid mass on rc-target response and damage
- Estimation of liquid mass passing the rc-target in cases with perforation of rc-targets

In total, ten tests with rc-slabs were performed to address these issues. Further, seven force plate tests were performed to verify design and predicted behaviour of the missiles as well as to measure LTF.

METHODS

Fundamental test parameters are listed in Table 1. Cylindrical thin walled (t=2 mm) stainless steel (EN 1.4432) pipes (Ø254 mm) with water infill were used as missiles (see Figure 1). The missile design with partially filled water tank was used in L2 and L5. To ensure a reliable splitting of the steel pipe, the fully filled missile design exhibits four rows of dents (Ø=3 mm, depths=0.8 mm) spaced at quartile points in longitudinal direction. In test L1 these dents are missing. However, it turned out that the effect on LTF of these rows is supposed to be small. All targets were two-way supported rc-slabs (C40/50) with outer dimensions of 2.1x2.1x0.15 m and a span width of 2 m, which is realised with cylindrical roller supports at

all edges and faces. Bending reinforcement is realised by B500B bars (Ø6 mm) with spacing of 50 mm each way and each face. In L1-L7 a shear reinforcement ratio of 53.5 cm^2/m^2 in form of closed shaped stirrups was used. This type of slab was tested in other test series of IMPACT related to bending failure due to soft missile impact. Despite a small difference in spacing of bending reinforcement it has been extensively studied in the IRIS benchmark hosted by OECD/NEA (2012). The slab is inserted in a steel frame and horizontally supported against the laboratory wall. Some details on the dimensions and target support are given in Figure 2. Tests L8-L10 were meant to address perforation or just-perforation of the slab and were performed without stirrups. In these cases, water passing the slab was collected in veneer-boxes (see Figure 14). Instrumentation included displacement transducers anchored in the concrete at the layer of rear-face reinforcement and high-elongation strain gauges glued to rear-face reinforcement bars. In addition to rc-slab tests seven tests with a steel plate target supported by load cells were carried out to measure impact forces. Force-plate test cases relevant for this paper are LFP2 (v_0=109.3 m/s) with a partially filled missile and LFP3 (v_0=107.6 m/s) with a fully filled missile.

Table 1: Basic test parameters (L2 and L5 with partially filled missile); total missile mass about 50 kg

Test	**L1**	**L2**	**L3**	**L4**	**L5**	**L6**	**L7**	**L8**	**L9**	**L10**
v_0 / m/s	112.9	111.1	137.5	147.3	138.4	117.7	168.9	113.7	166.7	131.8
M_{water}/ kg	39.2	26	37.8	37.6	26.0	38.0	38.4	38.3	38.2	37.8

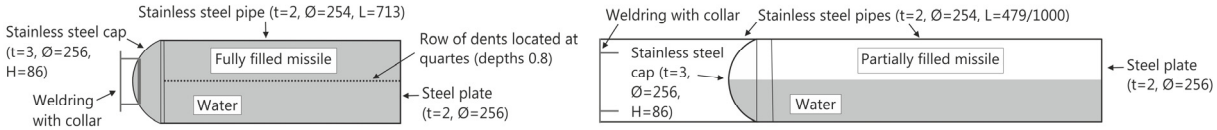

Figure 1. Measurements (in mm) of fully filled (left) and partially filled (right) missiles.

Numerical simulations of the tests were performed with LS-DYNA (LSTC (2020)) and ANSYS AUTODYN (ANSYS Inc. (2021)) using the RHT concrete model (Riedel and Borrvall (2011)). Figure 2 shows a setup of a numerical model. An average shell element size of 4.5 mm is chosen for structural parts of the missile. The model also includes the weakening dents and thus ensures the experimentally observed splitting mode, whereby a failure criterion of 25% effective plastic strain is used. Water is represented by the SPH (smoothed particle hydrodynamics) method, at which the particle size of 2.25 mm is chosen as half of the size of the surrounding elements. By means of a user-own subroutine tracking of trajectories of SPH particles is possible in AUTODYN simulations. This provides in principle a method to estimate the mass of water which perforates the target in tests L8-L10. With respect to computational costs, LS-DYNA was preferred in other cases. Further details on modelling of the target slab regarding mesh size, consideration of reinforcement and representation of frame are given in Heckötter and Sievers (2021).

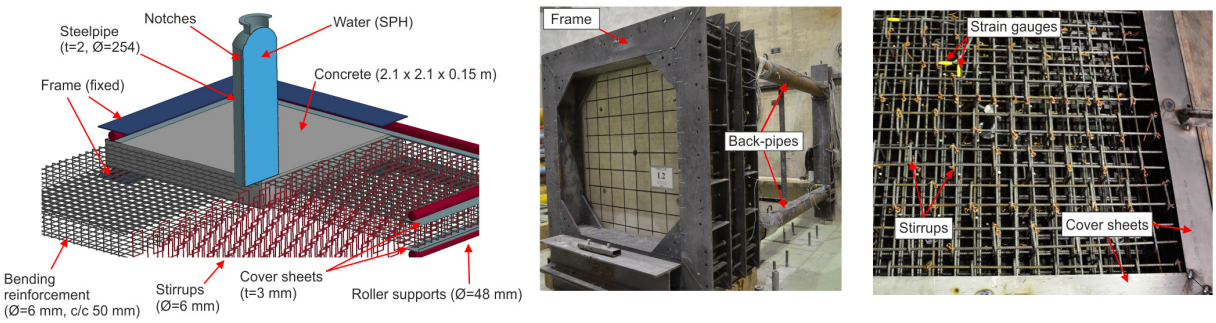

Figure 2. Details on analysis model and experimental setup.

INFLUENCE OF LIQUID INFILL ON LOAD-TIME-FUNCTIONS

Figure 3 compares the sum of load-cell-signals of selected force-plate tests and crushing behaviour of the missiles in LFP2 and LFP3. Test FP8 was performed with a soft missile with a total mass of 50 kg formed by a stainless-steel pipe (Ø254 mm) and a spherical nose segment at an impact velocity of 102.3 m/s. In FP8 buckling of the missile without any rupture occurs. In LFP3 immediate rupture of the pipe and radial release of water occurs. Due to the mass flow the impact forces during the first 4-5 ms are larger compared with LFP2 and FP8. In LPF2 the major amount of water is located in a segment close to the spherical cap (see Figure 1). Hence, buckling of the steel pipe occurs during the first 4-5 ms and impact forces in this time interval are quite similar to results of FP8. After about 5 ms the major amount of water mass arrives the force-plate and rupture of the pipe occurs. Since the water is somewhat confined in the folded segment of the pipe peak impact forces of LFP2 are larger than those of LFP3. Load-cell signals include inertia forces of the force-plate. Therefore, peak forces from load-cell signals are somewhat larger than actual impact forces. Some details on the force plate system and FP8 are given in Heckötter and Sievers (2015).

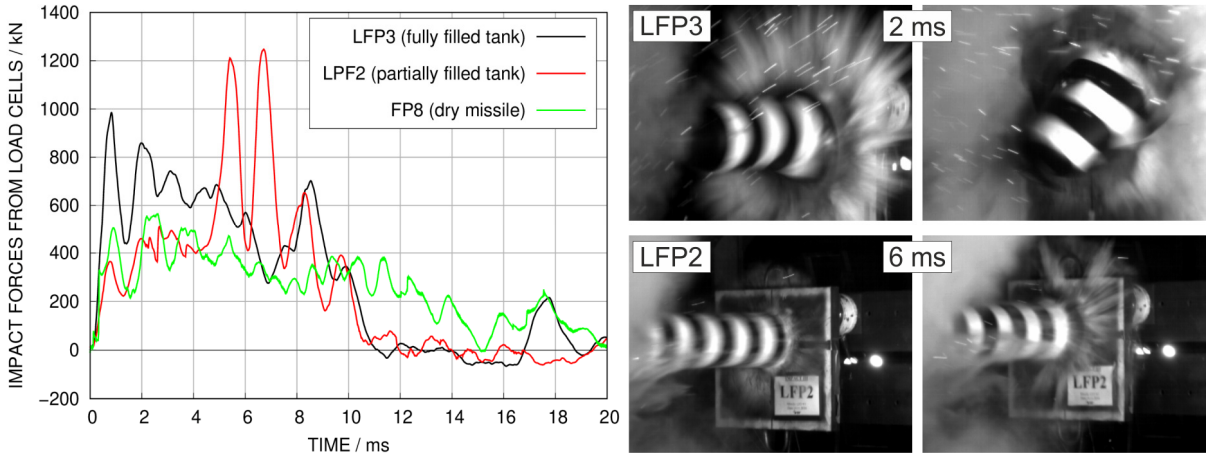

Figure 3. Selected force-plate test results on load-cell forces and crushing of missiles.

Figure 4 outlines a specific effect mentioned by Bowden and Field (1964) related to a liquid cylinder impacting a rigid wall. Due to the even contact surface the liquid initially behaves in a compressive manner. The peak force may be estimated according to Equation 1, at which c is the compressional wave velocity, ρ the fluid density and v the impact velocity. The duration of the initial peak is estimated by the time R/c taken for the release wave to travel from the outer surface to the axis of the cylinder.

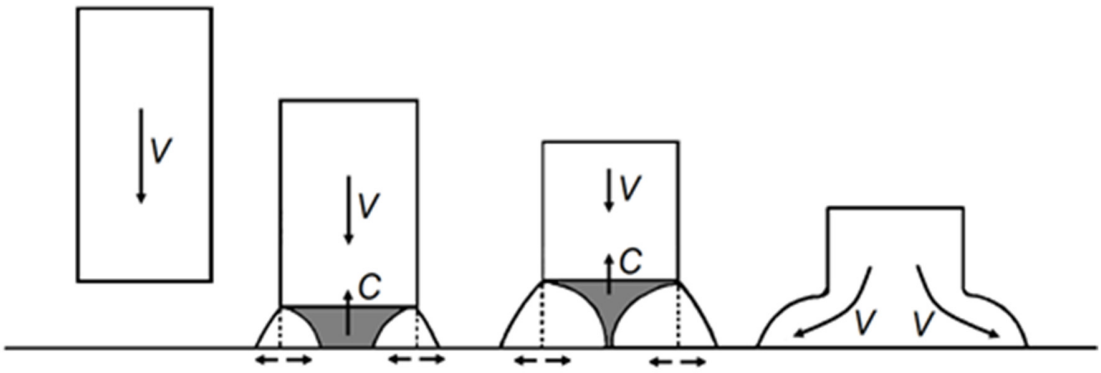

Figure 4. Initial compression during impact of a liquid cylinder according to Bowden and Field (1964).

$$F_{peak} = \pi R^2 \rho c v \quad (1)$$

In principle the SPH discretization is capable to reproduce the effect of initial compression. Figure 5 shows a sequence of pressure distributions of the cylindrical water part in section view calculated within an AUTODYN simulation of test L1. The process of pressure relief is completed within a time-interval of about 0.1 ms. In subsequent stages of impact, the pressure decreases to significantly lower values and a radial release of water occurs. In this context the radial velocity is about two times larger than the initial impact velocity and the spreading angle is quite flat. Similar findings are reported by Silde et al. (2009) for the initial stages of water release in another test series on liquid impact. However, effects of droplet size distribution and related drag phenomena cannot be reproduced by SPH.

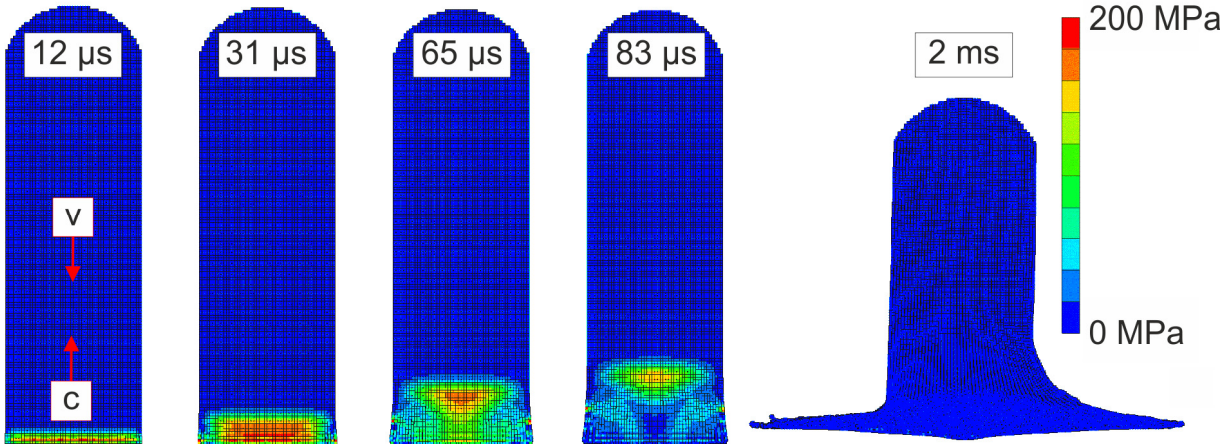

Figure 5. Initial compression of water cylinder in AUTODYN simulation of test L1.

Figure 6 compares numerical contact forces of an AUTODYN simulation of test L1 with results of the Riera (1968) method, at which the formula used to calculate the crushing force of a splitting pipe is documented elsewhere (Heckötter and Sievers(2015)). In this case the impact forces are predominantly determined by the mass flow of water. Regarding peak forces and shock duration results are consistent with force-plate test LFP3 (see Figure 3). Figure 6 includes also numerical results as well as an estimation according to Equation 1 on peak forces due to the initial compression effect. Notice, that initial peak forces of about 7-8 MN are substantially larger than the average force level of the subsequent impact and the duration of the initial peak is substantially smaller than the duration of impact.

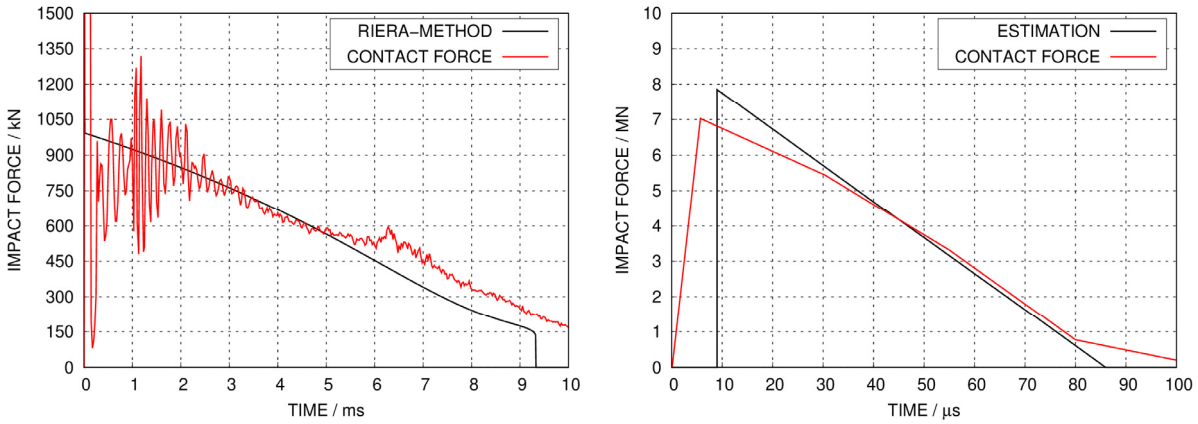

Figure 6. Contact forces and results of Riera-method (left), initial peak and estimation (right) for test L1.

RESPONSE OF REINFORCED CONCRETE SLABS

For test cases L1 and L2 Figure 7 compares central deflections at position of sensor D1 measured at the rear face of the slab as well as deflections at a sensor position D4 located on the diagonal 566 mm away from the centre. Further, photographs of the rear faces of the slabs are shown. Numerical simulations using LS-DYNA were performed for L1 only, since the crushing behaviour of the partially filled missile in L2 could not yet be satisfyingly reproduced in simulations. Scabbing of concrete in the centre occurred in both cases, but it is apparently much more pronounced in L1. Smaller displacements were measured in test L2, even though the peak of the LTF might have been larger in L1 (see Figure 3). This might be explained by the longer duration of water mass flow in L1 and by the effect of initial peak force. A steep increase of central deflection is visible in L1 test data and numerical result. This effect and the increased scabbing in L1 are attributed to the force peak caused by the initial compression of water. Due to sloshing of water inside the tank in L2 the water surface is not planar when it impacts the slab. Hence, no pronounced initial compression effect is visible in L2 results. Due to the offset of sensor location D4 to the loaded area, no steep increase of displacement caused by the initial force peak occurs. For sensor D1 the maximum and permanent elongations are overestimated by the simulation of L1, even though the maximum measured value is probably questionable. Regarding elongation and post impact vibration frequency numerical data satisfyingly reproduces the test result at location of D4, which indicates a realistic representation of damage.

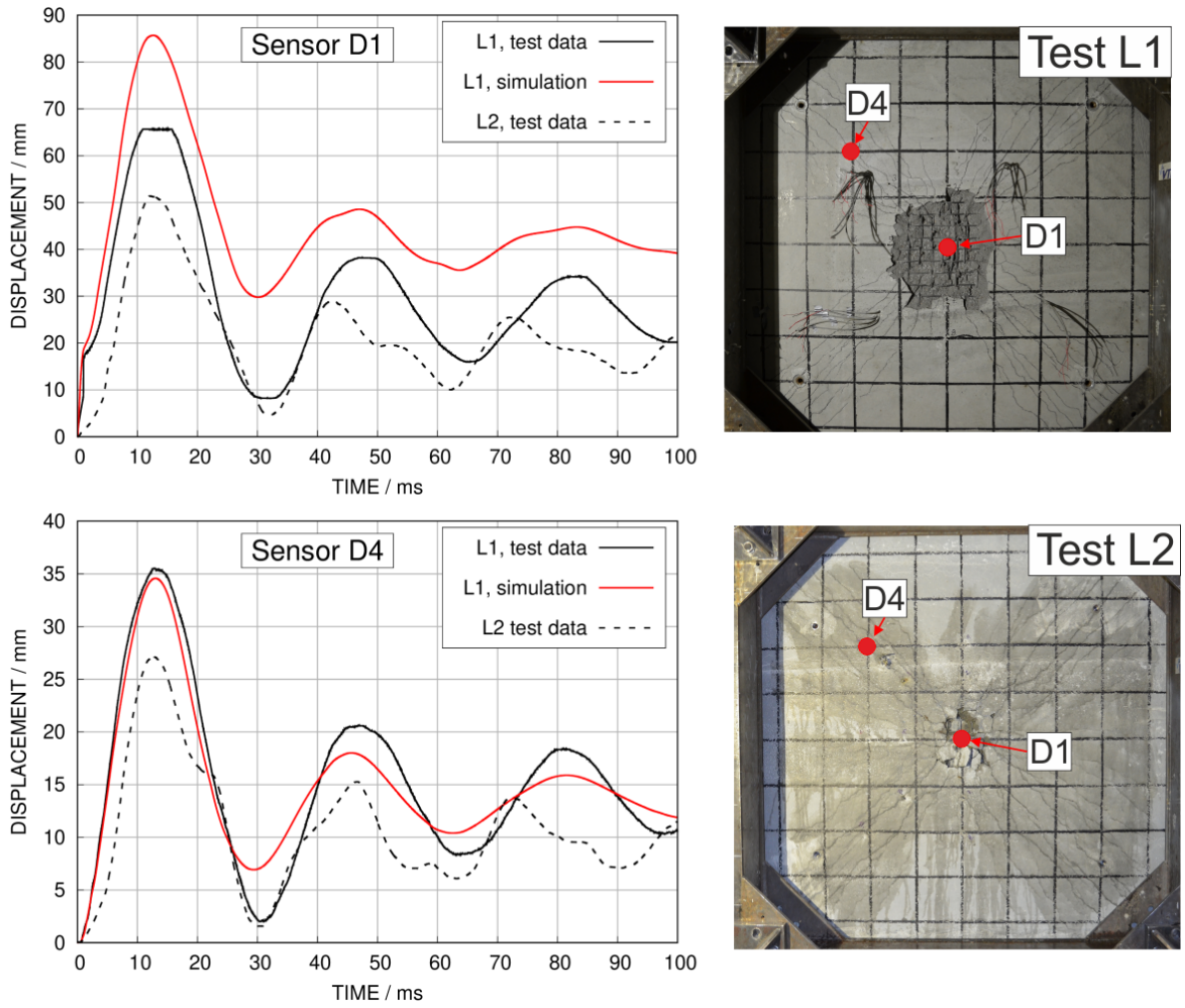

Figure 7. Comparison of rear face slab deflections and rear face damage in tests L1 and L2.

The effect of impact velocity is illustrated in Figure 8 with a comparison of front face damage. Numerical results display contour plots of the damage parameter of the RHT model. In this context a damage parameter of one corresponds to totally damaged material. In test L6 the damage is limited to the cross section of the missile and smaller regions located in the yield-lines. Due to the increased impact velocity the damaged area in the centre exhibits a diameter, which is larger than the diameter of the missile. In the photographs a corresponding circular crack is clearly visible. This type of damage is attributed to increase of loaded area during the radial water release and it indicates the formation of a punching cone. In principle the SPH method is suitable to reproduce this effect. Further, pronounced spalling of concrete is visible along the yield lines. This damage is associated with material failure in compression.

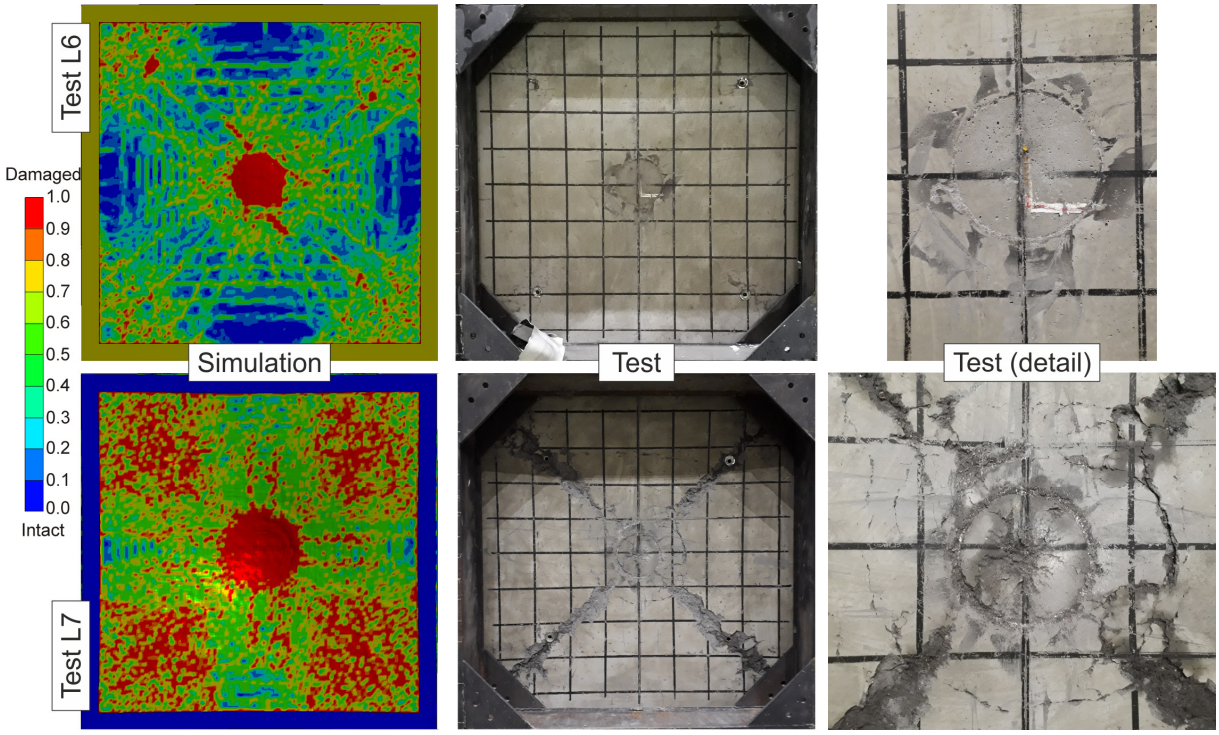

Figure 8. Front faces after tests L6 and L7 compared to damage contours in LS-DYNA simulations.

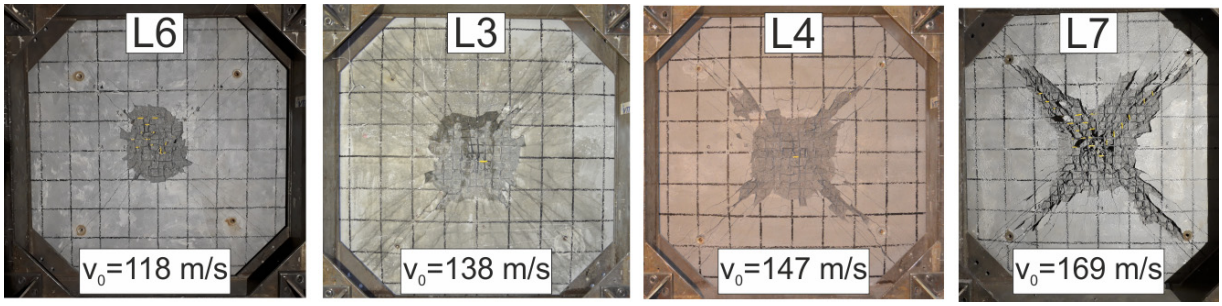

Figure 9. Post-test photographs of back faces with increasing impact velocity from left to right.

The effect of impact velocity on back face slab damage is illustrated in Figure 9. An increase of extend of scabbed area is notable when comparing L6 and L3. Further increase of impact velocity results in pronounced damage along the yield-lines. Figure 10 presents comparative plots of time histories for displacements and reinforcement strains for tests L6 and L7. Test L6 was carried out with a repetition of L1, using the missile design with notches and a revised layout of strain gauges. In both cases the displacement transducers are located on the diagonal 566 mm distant from the centre. In L6 the strain gauge

is close to the position of displacement measurement. Unfortunately, many strain gauges got broken during test L7, therefore results of the most adjacent strain gauge are presented for this case. It is apparent, that strains and displacements are in phase for test L6. This indicates a bending vibration of the slab. Similar evaluations indicated bending as the predominant failure mode for L3 and L4. For test L7 it seems, that strains and displacements are not in phase. In combination with the observed slab damage this indicates a combined bending and punching failure of the slab. Figure 11 exemplarily compares numerical results and test data on maximum strains for test L6. Reinforcement strains reach values up to 10%. They are probably due to local dents of reinforcement bars found in tests more difficult to simulate than slab displacements.

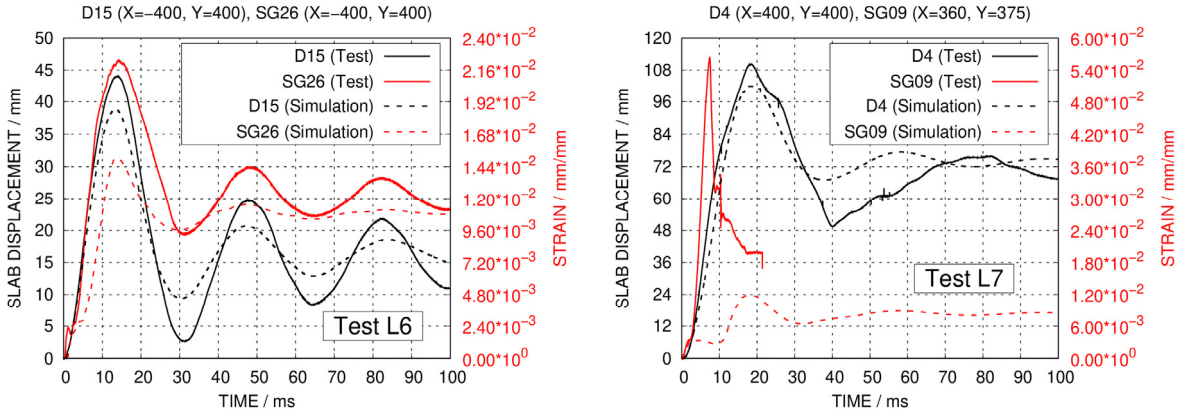

Figure 10. Comparison of selected slab displacements and reinforcement strains in L6 and L7.

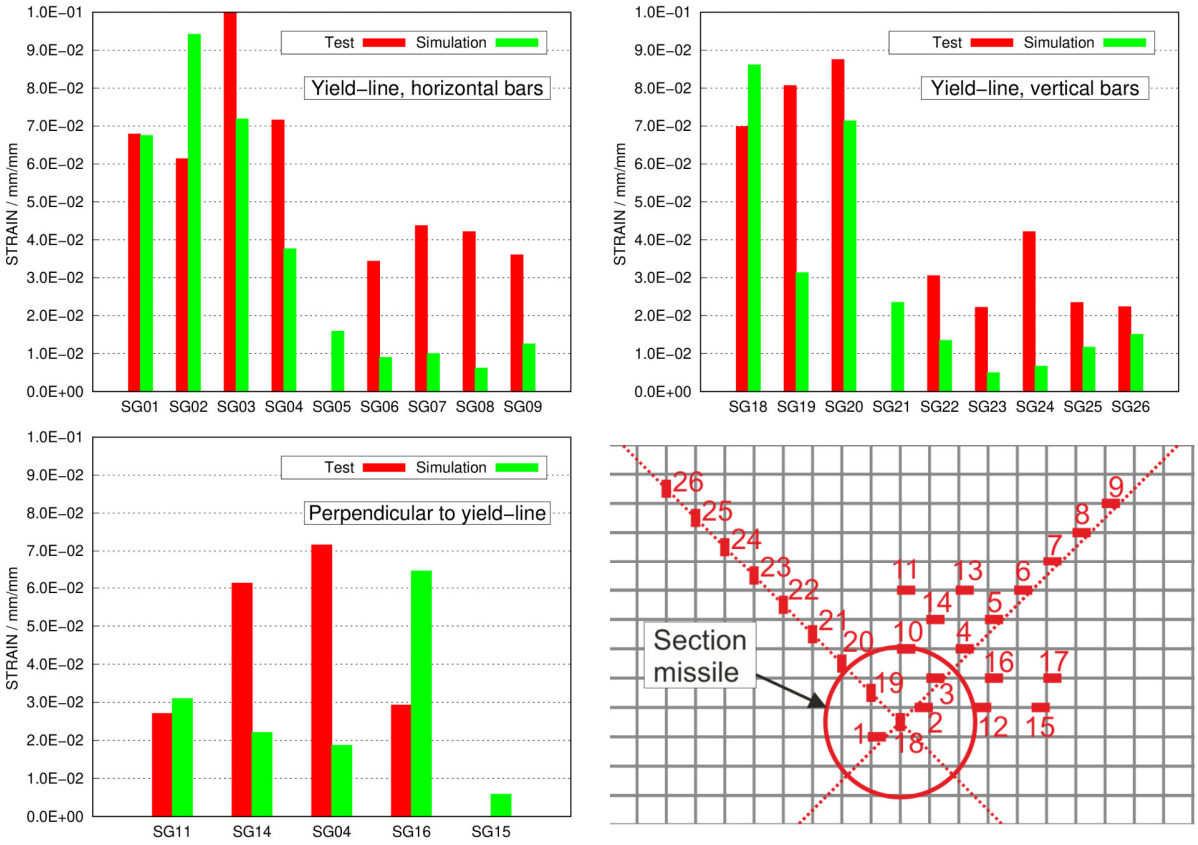

Figure 11. Selected maximum reinforcement strain values in test L6 compared to LS-DYNA results.

SLAB PERFORATION AND DEPOSITION OF WATER

Another objective of the L-series was to demonstrate the possibility of water deposition behind the slab and to quantify the mass of water passing the slab. Therefore, tests L8-L10 were performed without shear reinforcement. The anticipated failure mechanisms were just perforation for L8 and perforation for L9 and L10. Figure 12 compares post-test photographs taken from the back faces with contours of the damage parameter of the RHT model in AUTODYN simulations. In L8 concrete is destroyed over the full slab thickness. Loose concrete is retained by the plastically deformed but unbroken reinforcement. In the lower region of the damaged area some water flow is visible, but no deposition of water on the rear face is found. In contrast to this the slab is perforated in test L9 and a significant amount of water is deposited on the rear face. Since plastic bags located behind the slab were destroyed by debris, a collection of deposited water was not possible. An evaluation of high-speed camera frames indicates that probably 50 % of the water infill of the missile perforated the slab. The diameter of the hole is larger than the missile diameter. This effect is related to the increase of loaded area due to radially release of water and in principle captured by the SPH method. Perforation occurred in L10 and a certain flow of water in the lower region of damage is noted. Due to a lower impact velocity and a strengthened collection system (see Figure 14) consisting of a veneer box cladded with plastic sheets, collection of deposited water was possible in L10. According to a rough estimation, 7.9 kg of water were deposited on the rear face. The water mass spent for rehydration of debris was estimated by means of differential weighing of wet and dry debris. In principle the AUTODYN simulations are capable to reproduce the concrete damage. Horizontal reinforcement bars are located close to the surface. Hence, the damage is asymmetric and somewhat larger in horizontal direction. Due to the refined modelling including separation of vertical and horizontal reinforcement, the simulations are capable to reproduce this effect. Differences regarding number of broken reinforcement bars remain. These are sensitive failure criteria of reinforcement steel. Due to localisation of rupture, smaller values than failure strains obtained in tensile tests should be used. This study uses 10 % of effective plastic strain.

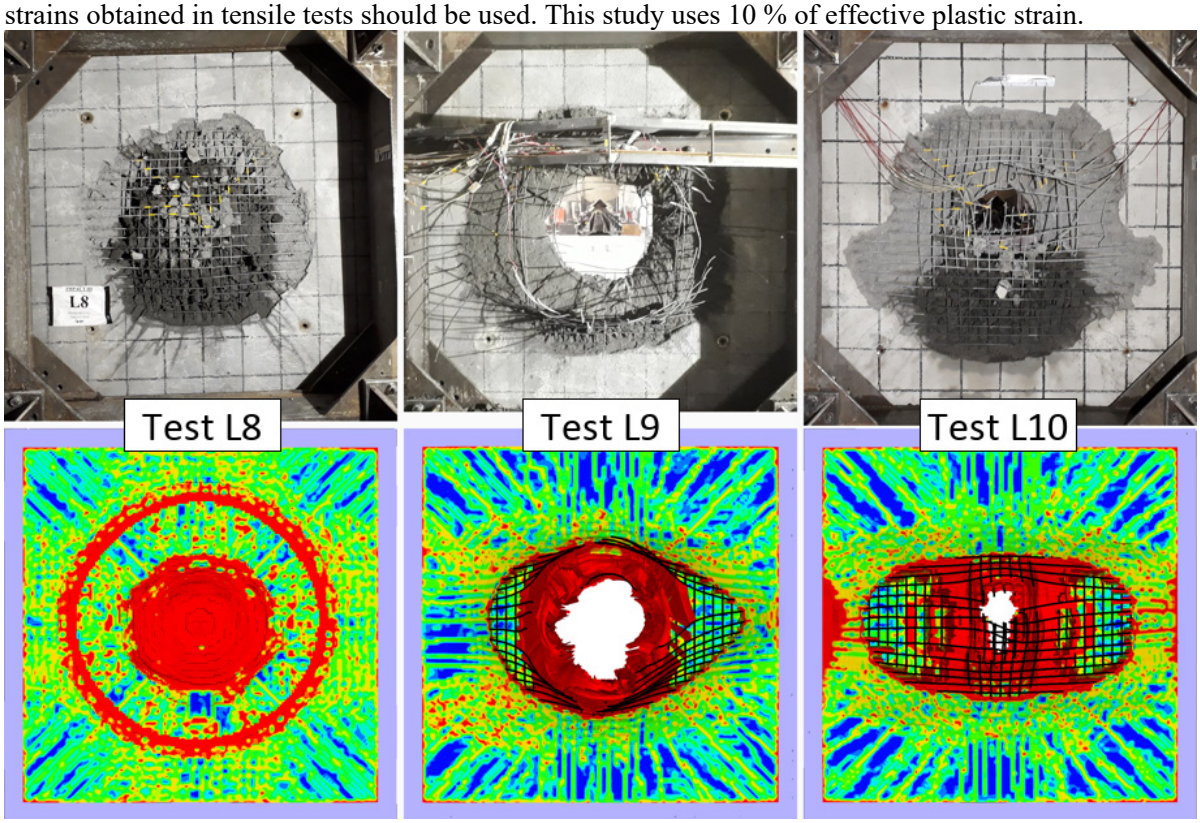

Figure 12. Back faces tests L8, L9 and L10 compared to damage contours in AUTODYN simulations.

A sequence of model section views in an AUTODYN simulation of test L10 is shown in Figure 13. Water is radially released from the missile and spread under a flat angle in front of the slab. However, a certain amount of water penetrates the slab. Failure criteria of several reinforcement bars are exceeded, and the slab is not able to retain a certain amount of water that travels into the direction of initial velocity. Therefore, a certain mass of water will pass a defined control plane which is located behind the slab. By means of a user-own subroutine in AUTODYN the trajectories of SPH particles are tracked to estimate the spatial distribution of water. Time histories of water masses in the three regions mentioned above are displayed in Figure 14. A very small fraction of water enters the rear face in L8, while more than 15 kg perforate the slab in L9. The result on perforated water mass for L10 is within the uncertainty range of the test. Given all uncertainties in simulations and measurement the results are supposed to be satisfying.

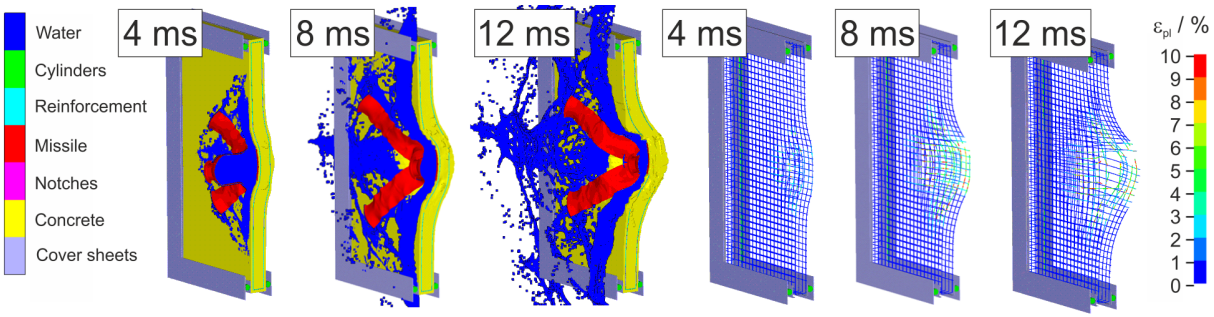

Figure 13. Sequence of model deformation and reinforcement strain in AUTODYN simulation of L10.

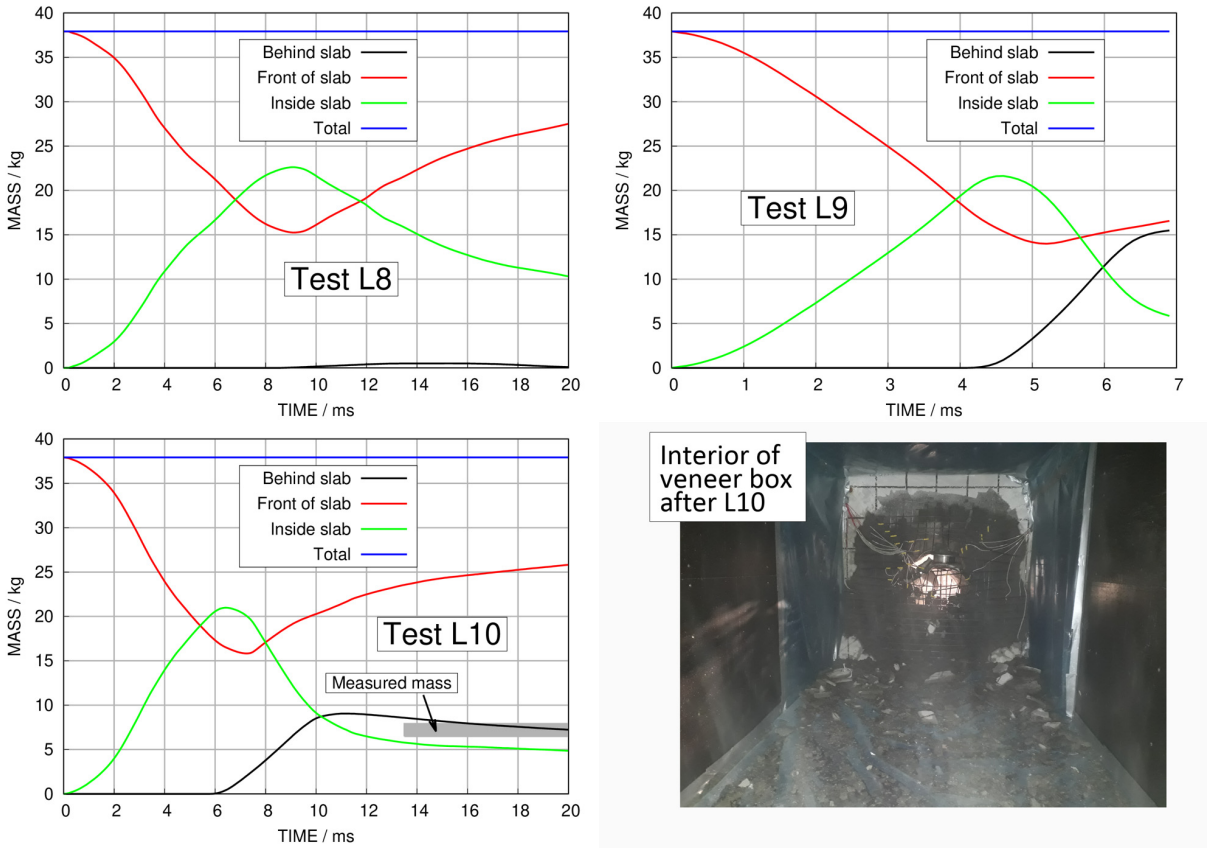

Figure 14. Results of AUTODYN simulations on water deposition in tests L8, L9 and L10.

CONCLUSION

An initial peak-like pressure pulse due to the impacting water column is visible in measured slab displacements and increased detachment of scabbed concrete in the centre. This effect is reproduced by numerical simulations and not observed for tests with partially water-filled missiles.

Due to deposition of water the loaded area is larger than the diameter of the missile, which is visible in punching cone geometries and diameter of holes. In numerical simulations such effects may be reproduced using SPH discretization of the liquid, which includes time dependent variation of the loaded area by means of contact.

The tests confirmed that liquid may pass the slab. It was possible to roughly estimate the water mass perforating the slab in test L10. In principle SPH-simulations are capable to quantify the perforating mass of water. The safety related relevance of this estimation is given by the quantification of potential thermal loading due to kerosene fire as subsequent event in an airplane crash scenario.

ACKNOWLEDGEMENT

The work of GRS was carried out in the frame of the German reactor safety research program funded by the German Federal Ministries for Economic Affairs and Climate Action (BMWK) and for Environment, Nature Conservation, Nuclear Safety and Consumer Protection (BMUV).

REFERENCES

Ansys Inc. (2021). “AUTODYN Version 2021 R1 - Explicit Software for Non-Linear Dynamics.” USA.

Borrvall, T., Riedel, W. (2011). “The RHT Concrete Model in LS-DYNA,” *8th European LS-DYNA Conference*, Strasbourg, France

Bowden, F.P., Field, J.E. (1964). “The brittle fracture of solids by liquid impact, by solid impact, and by shock,” *Proceedings of the Royal Society London A 282*, 331–352.

Heckötter, C., Sievers, J. (2015). “Impact of different sized deformable projectiles with and without liquid filling,” *Transactions of SMiRT 23,* Division IV, Manchester, United Kingdom.

Heckötter, C., Sievers, J. (2021). “Numerical Analysis of Impact Tests on Bending Failure of Reinforced Concrete Slabs Subjected to Inclined Soft Missile Impact,” *13th European LS-DYNA Conference*, Ulm, Germany.

Hessheimer, M.F., Dameron, R.A. (2006). “Containment Integrity Research at Sandia National Laboratories,” NUREG/CR-6906.

Lastunen, A., Hakola, I., Järvinen, E., Calonius, K., Hyvärinen, J. (2007). “Impact Test Facility,” *Transactions of SMiRT 19*, Toronto, Canada.

LSTC (2020). “LS-DYNA, A Program for Nonlinear Dynamic Analysis of Structures in Three Dimensions”, Version R12.0, Livermore Software Technology Corporation.

NEA (2012). “Improving Robustness Assessment Methodologies for Structures Impacted by Missiles (IRIS_2010),” *Final Report,* NEA/CSNI/R(2011)8, Nuclear Energy Agency.

Riera, J.D. (1968): “On the Stress Analysis of Structures Subjected to Aircraft Impact Forces," *Nuclear Engineering and Design 8,* 415-426.

Silde, A., Kankkunen, J., Juntunen, J. (2009). “Study of Liquid Dispersal from a Missile Impacting a Wall,” *Transactions of SMiRT 20,* Division 5, Espoo, Finland

Tarallo, F., Rambach, J.-M. (2013). “Some Lessons Learned from Tests of VTT IMPACT Program, Phases I and II,” *Transactions of SMiRT 22,* San Francisco, USA, 2013

VTT (2019). “IMPACT III: water-filled projectile tests,” *Research report VTT-R-00265-19,*confidential.